Journal of Nanoscience & Nanotechnology Research

Open Access Review Article

Nanoparticles Reactions in Cervical Cancer: Challenge and Hope

V Anusha Devi[1*], Kalaiselvi V[2]

[1]*Department of Physics, Nandha Arts and Science College, Tamilnadu, India*

[2]*Department of Physics, Navarasam Arts and Science College for Women, Tamilnadu, India*

ABSTRACT

In this paper, a co-precipitation and thermal breakdown approach was used to create a CuO/SnO nanocomposite using CuO, NiO, and SnO as precursors. Sol-gel synthesis was used to create Nickel Oxide (NiO) nano-particles. The XRD (X-Ray Diffraction), SEM (Scanning Electron Microscopy), and FTIR (Fourier Transform Infrared Analysis) were used to analyze the nanocomposites as-prepared; CuO and SnO have wurtzite crystal structures that are cubic and hexagonal, respectively, as seen by the XRD diffractogram of a CuO/SnO nano-composite. The existence of CuO and SnO was verified by FTIR bands in the CuO/SnO nano-composite. The concept of CuO nano-particles mixed with *Hibiscus* flower reacted as anti-cancer property.

Keywords: Nano-composite; CuO; SnO; NiO; FTIR; XRD; *Hibiscus* flower; Anti-cancer study

INTRODUCTION

Two of the major drivers of pollution and energy consumption are population growth and rapid urban/industrialization. By discharging polluted and coloured effluent into the water supply, synthetic organics used in industries like medicines, textiles, cosmetics, paper, and plastics have seriously harmed the environment. They degrade water quality, impede light penetration, and reduce photosynthetic responses. Furthermore, certain colours are both toxic and carcinogenic. The aforementioned issues have been dealt with using a variety of therapeutic techniques. In treatment procedures such as adsorption, chemical precipitation, and coagulation are inefficient and produce secondary pollutants such as hazardous gases and slurry, which require extra purification. As a result, innovative technology based methods for pollution removal have been proposed.

Advanced Oxidation Processes (AOPs) have received a lot of interest as a replacement for existing treatment approaches for converting hazardous organic pollutants into innocuous chemicals. AOPs have benefits including the ability to function at normal temperatures and pressures and convert environmental contaminants into sustainable products. The energy levels of these semiconductors are essentially the same. In contrast, SnO is easily accessible, absorbs a sizeable amount of solar energy, and has higher photo catalytic activity than TiO_2.

Due to their exceptional characteristics, such as low cost, photoconductive response, pyro electricity, and surface fictionalization, high binding energy, and electron transfer efficiency, zinc oxide based materials are used in multifunctional electrode applications such as dye sensitized solar cells, lithium ion batteries, gas sensors, air quality

Received:	03-December-2022	**Manuscript No:**	IPNNR-22-15229
Editor assigned:	06-December-2022	**PreQC No:**	IPNNR-22-15229 (PQ)
Reviewed:	20-December-2022	**QC No:**	IPNNR-22-15229
Revised:	20-September-2023	**Manuscript No:**	IPNNR-22-15229 (R)
Published:	27-September-2023	**DOI:**	10.12769/IPNNR.23.7.022

Corresponding author: V Anusha Devi , Department of Physics, Nandha Arts and Science College, Tamilnadu, India; E-mail: anugee20@gmail.com

Citation: Devi VA, Kalaiselvi V (2023) Nanoparticles Reactions in Cervical Cancer: Challenge and Hope. J Nanosci Nanotechnol Res. 7:22.

monitoring. These materials are likewise inexpensive, inexpensive, and This metal oxide based semiconductor is used in several different optoelectronic technologies, including light emitting diodes, flat panel displays, transparent semiconductors, and conductive oxides, due to its exceptional optical properties [1-5].

The studies have examined the use of SnO based materials for sensing and photovoltaic applications, including the detection of ammonia gas using Ag/SnO flowers and Cu doped SnO nanostructures, the detection of NO_2 gas using tiSnO thin films, the detection of ethanol vapour using SnO. In $2O_3$ core shell nanofibers, and the development of quaternary transparent conductive oxide materials lithium ion batteries have proven a major success in little electrical devices.

To create pure NiO nanoparticles, it is necessary to regulate the solution's pH level, structure, and calcinations temperature. These factors have an impact on the particles' shape, size, and dispersion. If pure NiO is created, its precise physical and chemical characteristics can be identified. Because of its superior crystalline, uniform particle dispersion, homogenous mixing, and smaller particle size, the sol gel process is a good choice for making NiO nanoparticles [6].

The use of lithium in massive electrical energy storage devices is nonetheless constrained by the dearth of lithium minerals. Layered sodium transition-metal oxides are promising materials that can significantly aid in the development of large scale electrical energy storage devices by reducing the issues associated with lithium batteries due to their exceptional cycle stability and rate performance [7].

SnO, on the other hand, has large bandgap energy and only absorbs electromagnetic radiation in the UV area. Because just 3%-5% of the solar energy's Ultraviolet (UV) component reaches the earth, its photo catalytic activity under solar radiation is limited. In order to increase the photocatalytic activity of existing photo catalysts like SnO, doping or co-doping with metals and nonmetals is currently being used. Additionally, exchanging charge carriers amongst several nanostructured semiconductors enhances photo catalytic performance [8].

Consequently, there were national strategies for the evaluation of the clinically relevant nanoparticle presentations. We want to highlight the function and efficiency of nanoparticle usage in cancer treatment. In this review, as well as the significance of toxicity testing for this novel strategy (**Figure 1**).

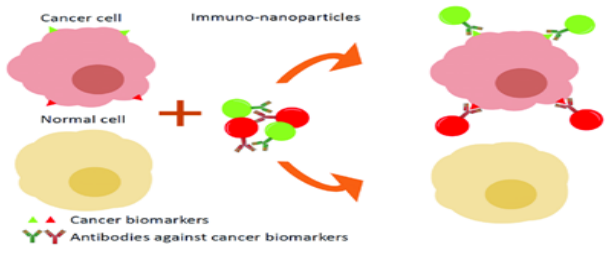

Figure 1: A good illustration of the distinction between passive and active nanoparticles in cancer tissue.

As a photocatalyst for visible light, Cuprous Oxide (CuO), a tapered band gap semi-conductor, has been proposed. Using the energy from visible light, electrons in CuO can transition from the valence band to the conduction band. However, after being formed, electrons and holes generated by lasers mix fast, which might harm the photocatalytic activity. The CuO has previously been combined with grapheme and other metals to prevent photo induced electrons and holes from recombining. It is anticipated that CuO will be employed in tandem with high band gap metal oxides, such as SnO, as an operational strategy to address the charge carrier recombination issue. In this work, a CuO/SnO nanocomposite was made using co-precipitation and thermal breakdown procedures in the eradication of the model dye pollution methyl red (**Figure 2**) was examined.

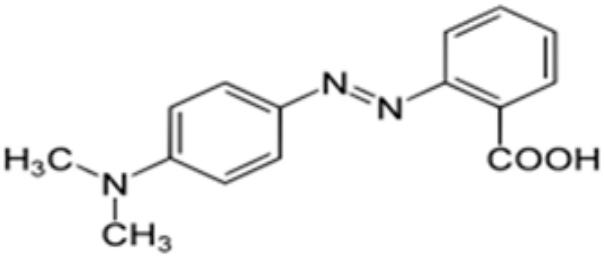

Figure 2: Structure of methyl red.

It ranks as the third most frequent cancer among women and the fourth most frequent reason for cancer related mortality. 16,710 new cases, or 16.35 occurrences per 100,000 women, are anticipated in 2022. With a mortality rate of 5.33 per 100,000 women, Cervical Cancer (CC) claimed 6,627 lives in the nation in 2020. In 2019, CC resulted in a loss of 160.8 DALYs.

MATERIALS AND METHODS

Experimental Study

Sample preparation: The chemicals used included metal oxides, solvent NaoH, copper, nickel, and tin chlorides. The sol gel approach made use of analytical grade chemicals. Distilled water was used in every experiment. The 1 M tin chloride was mixed with 30 ml water. 1 M NaOH was mixed with 30 ml water in the same way. Then, drop by drop, add the NaOH solution to the tin chloride solution. After 20 minutes of stirring, gel formation was obtained. Then place it in the microwave oven at the temperature specified. Then, obtain powder and thoroughly mill it to obtain nano powder.

Characterization techniques: The crystal structures and average crystallite size of the samples were determined using an XRD (Shimadzu XRD-7000, Shimadzu corp., Kyoto, Japan) in phase scan mode with Cu-K radiation (=0.15406 nm), phase time and degree (2) of 0.4 s and 0.02 s, accordingly, for the range of 10 to 80. The surface morphology of the materials was examined using a JEOL JSM-5610 Scanning Electron Microscope (SEM) with an Everhart-Thornley detector (JEOL, Ltd., Akishima, and Tokyo). Utilizing KBr pellets and an FT-IR spectrum 65

(PerkinElmer, Waltham, MA, USA) in the 4000 cm^{-1}-400 cm^{-1} range, the chemical makeup of the generated samples was determined. The absorption spectra were estimated using the Kubelka-Munk method, and the properties of the nanocomposites were examined using a PerkinElmer Lamda 35 spectrometer with a 200 nm-800 nm wavelength range [9-14].

RESULTS AND DISCUSSION

XRD Analysis

The nano-particle diffraction pattern is consisting of CuO, SnO, CuO/SnO, and CuO/SnO are shown in **Figure 3**. Similar results were reported by diffraction peaks of SnO, and CuO/SnO, nanomaterial's found in XRD patterns at 2=31.76, 34.40, 36.24, 47.53, 56.59, 62.85, 66.37, 67.90, and 69.07, which correspond to the (100), (002), (101), (102), (110), (103), (200), (112). According to Jiang, et.al., the cuprous oxide XRD patterns diffraction peaks at 2 values of 29.57, 36.40, 42.32, 61.43, 73.55, and 77.40 are reflections from the (110), (111),(200), (220), (311) and (222) crystal planes. XRD was used for further investigation to validate the phase of the produced NiO nanoparticles. The material was in an amorphous phase prior to calcinations, and no NiO phase was seen. All of the NiO diffraction lines were indexed to an ordered structure in the cubic structure that the crystalline phase displayed after the calcinations. All of the diffraction peaks at (111), (200),(220), (311), and (222) were seen at the crystalline phase.

The absence of additional diffraction peaks caused by contaminants like CuO, Cu (OH), demonstrates the purity of the nanostructured materials. **Figure 1** demonstrates that doping did not produce an additional peak, suggesting that the SnO and CuO lattices. The little shift in the NiO nanocomposite's diffraction peaks.

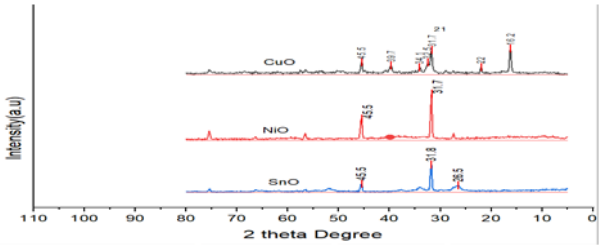

Figure 3: X-ray diffract gram of CuO, NiO and SnO of nano-materials.

The scherer equation was used to determine the typical nanomaterial crystallite sizes from the strong peak. Here, D stands for maximum size at full width, wavelength, bragg angle, and crystallite size in radians. Crystallite diameters for SnO, CuO, and NiO were reported to be 33.72 nm, 32.33 nm, and 13.57 nm, respectively. Considering these outcomes, nanocomposite has smaller crystallite sizes than CuO and SnO. The fact that NiO nanocomposite crystallite size is smaller than CuO and SnO nano-level particles may be due to the disruption of particle formation caused by CuO and SnO lattices.

SEM Analysis

As seen in the use of SEM was examining the surface morphology of nanomaterials made of CuO, SnO, and NiO. According to SEM micrographs, SnO has some agglomerated nanoparticles with an irregular shape, which is in line with. But SEM images of CuO, SnO, and NiO samples showed that they were reasonably organized and that there were much less particle agglomerations than in SnO nanoparticles with truncated octahedron shaped nanocrystals; this could be because CuO was present (**Figure 4**).

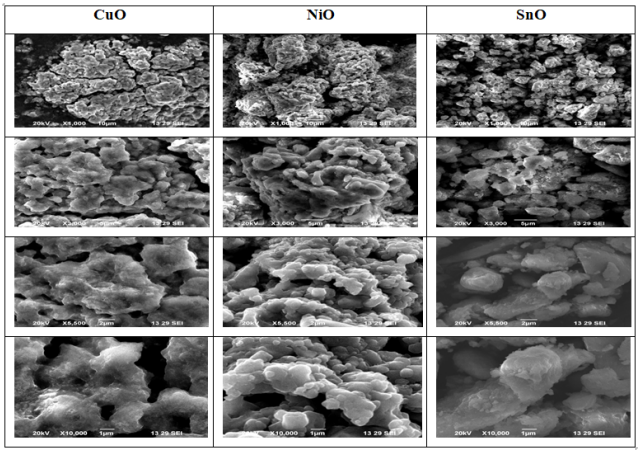

Figure 4: Scanning Electron Microscopy (SEM) morphology of nanomaterials.

FTIR Analysis

The FTIR bands of CuO, SnO, and NiO nano-materials are shown in **Figure 3**. With the exception of CuO, all materials showed peaks that appeared in the 490 cm^{-1}-505 cm^{-1} regions. These peaks correlate with the stretching vibration of SnO and match up with earlier studies. Peaks in the FTIR spectra of CuO, SnO, and NiO nanoparticles were observed and match the stretching vibration of CuO, with peaks in the region of 610 cm^{-1}-630 cm^{-1}; a related discovery was reported by the N-H stretching vibration mode may be the cause of the peak at 3169 cm^{-1} in the FT-IR spectra of the NiO nano-composite. An N-H bending vibration mode may be the source of the band at 1441 cm^{-1}. The FT-IR spectra of the CuO/SnO nano-composite showed the aforementioned absorption bands in addition to a peak at 431 cm^{-1}, which may be caused by the stretching vibration since similar results have been reported. As a consequence, the bands demonstrated that the NiO nanocomposite included SnO, CuO, and NiO (**Figure 5**) [15].

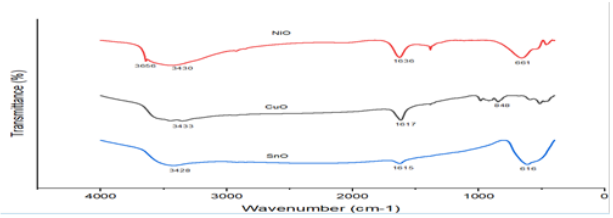

Figure 5: Fourier Transforms Infrared (FTIR) spectrums of CuO, SnO, and NiO nanomaterials.

Cell Procession

The HeLa (human cervical cancer cell line), which was grown in eagles least essential medium with 10% foetal bovine serum, was given by the NCCS (National Centre for Cell Science), Pune. The conditions for the cells' maintenance were a constant 370°C, 5% CO_2, 95% air, and 100% relative humidity. Maintenance cultures were tested every week, and the culture medium was changed twice a week [16].

Process for Treating Cells

The monolayer cells were separated into individual cell suspensions using EDTA acid (Trypsin-ethylenediaminetetraacetic acid), and viable cells were measured using a hem cytometer. Then, using medium containing 5% FBS, the specific cell suspensions were diluted to a final cell density of 1×10^5/ml. 10,000 cells in 100 micro liters of cell solution were seeded on 96 well plates, and they were incubated to encourage cell adhesion at 370°C, 5% CO_2, 95% air, and 100% relative humidity. After a 24 hour period, increased dosages of the test substances were administered to the cells. In the following step, a sample solution was created and diluted using serum free medium to double the required final maximum test concentration. To spread them, they were originally welcomed into Phosphate Buffered Saline (PBS). To produce a total of five sample concentrations, four further serial dilutions were carried out. These different sample dilutions were added to the appropriate wells that already had 100 l of medium in order to produce the necessary final sample concentrations. The plates were incubated for 48 hours after the sample was added at 37°C, 5% CO_2, 95% air, and 100% relative humidity. For each concentration, three duplicates were retained, and the control medium was used [17].

MTT Assay

3-[4, 5-dimethylthiazol-2-yl] yellow, water soluble tetrazolium salt 2,5-diphenyltetrazolium bromide (MTT). The mitochondrial enzyme succinate dehydrogenase breaks the tetrazolium ring, converting the MTT into an insoluble purple formosan. Thus, the quantity of formosan generated and the number of viable cells is directly correlated. Each well received 15 l of MTT (5 mg/ml) in Phosphate Buffered Saline (PBS), which was added, and was then incubated at 370°C for 4 hours a ter the initial 48 hours of incubation. When the MTT medium was stopped, the formosan crystals were dissolved in 100 l of DMSO, and the absorbance at 570 nm was then quanti ied using a micro plate reader. The formula below was used to determine the percentage of cell inhibition [18-20].

% Cell Inhibition=100-Abs (sample)/Abs (control) × 100.

The IC_{50} was determined by creating a nonlinear regression graph between the percentage of cell inhibition and the log concentration using the graph pad prism tool (**Table 1**, **Figures 6 and 7**).

Table 1: Data for MTT Assay

HeLa	Conc.	6.25 µg	12.5 µg	25 µg	50 µg	100 µg	Cont		
E 01	ABS	0.531	0.525	0.33	0.237	0.032	0.607	IC_{50}	33.54 µg/ml
		0.566	0.489	0.367	0.248	0.037	0.596		
		0.559	0.503	0.359	0.244	0.054	0.587	R^2	0.977
	Avg	0.552	0.507	0.352	0.243	0.041	0.596		
	% Cell inhibition	7.486	15.251	41.005	59.273	93.128			

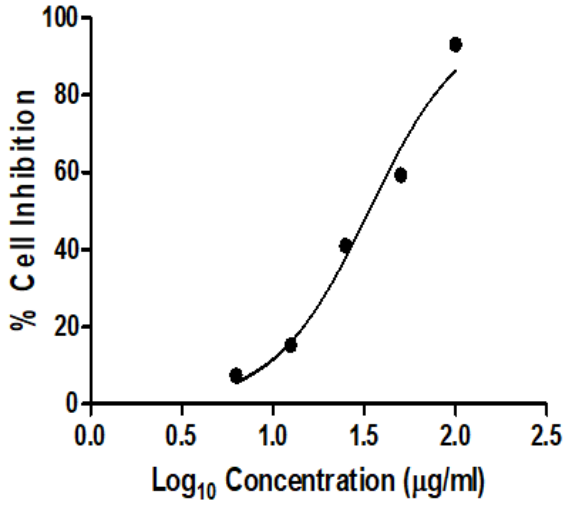

Figure 6: Data for MTT Assay.

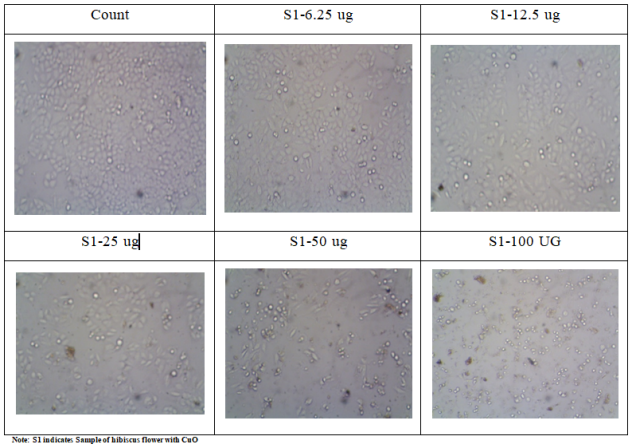

Figure 7: Plots for MTT Assay.

CONCLUSION

The fabrication of a CuO/SnO nano-composite used co-precipitation and thermal breakdown techniques. The NiO nanoparticles were successfully synthesized through the sol gel method. Thermal analysis was used to estimate the NiO nanoparticles' ideal calcinations temperature. The NiO nanoparticles developed a cubic structure. The sample demonstrated that no impurities were present, just pure NiO nanoparticles. The nanoscale range of the morphological analysis was proved, and NiO elements were effectively identified. In comparison to SnO, CuO, and CuO/SnO nanoparticles, the absorption edge of the nanocomposite was more extended to the visible range of electromagnetic radiation. Connection of CuO and SnO semiconductors, which may lower charge carrier recombination rates and boost solar absorption and use, is responsible for the improvement. CuO, NiO, and SnO nanocomposites showed MIC_{90} antifungal activity in a research against vaginal isolates of *C. albicans*. Cervical cancer is still a severe illness in less developed nations and regions, where effective preventative efforts still face considerable obstacles. The disease burden has fallen dramatically in industrialized countries and regions over the past several decades, but it is still a problem there. Various cost effective and scientifically supported preventative and control techniques are already available to fulfill the demands of regions with varying economic levels.

REFERENCES

1. Agarwal H, Kumar SV, Rajeshkumar S (2020) Antidiabetic effect of silver nanoparticles synthesized using lemongrass (*Cymbopogon citratus)* through conventional heating and microwave irradiation approach. J Microbiol Biotech Food Sci. 9(6):371-376.
2. Al-Zoubi MS, Aljabali AA, Pal K (2021) Highly toxic nanomaterials for cancer treatment. Bio man Nano. 18:161–185.
3. Alomari G, Al-Trad B, Hamdan S, Aljabali A, Al-Zoubi M, et al. (2020) Gold nanoparticles attenuate albuminuria by inhibiting podocyte injury in a rat model of diabetic nephropathy. Drug Deliv Trans Res. 10 (1):216–226.
4. Al-Trad B, Alkhateeb H, Alsmadi W, Al-Zoubi M (2019) Eugenol ameliorates insulin resistance, oxidative stress and inflammation in high fat diet/streptozotocin induced diabetic rat. Life Sci. 216:183-188.
5. Arvanag FM, Bayrami A, Yangjeh AH, Pouran SR (2019) A comprehensive study on antidiabetic and antibacterial activities of ZnO nanoparticles biosynthesized using *Silybum marianum* L seed extract. Mater Sci Eng C. 97:397–405
6. Balcha A, Yadav OP, Dey T (2016) Photocatalytic degradation of methylene blue dye by zinc oxide nanoparticles obtained from precipitation and sol-gel methods. Environ Sci Pollut Res. 23:25485–25493.
7. Behnajady M, Modirshahla N, Hamzavi R (2006) Kinetic study on photocatalytic degradation of CI acid yellow 23 by SnO photocatalyst. J Hazard Mater. 133:226–232.
8. Benedix R, Dehn F, Quaas J, Orgass M (2000) Application of titanium dioxide photocatalysis to create self-cleaning building materials. Lacer. 5:157–168.
9. Bora LV, Mewada RK (2017) Visible/solar light active photocatalysts for organic effluent treatment: Fundamentals, mechanisms and parametric review. Renew Sustain Energy Rev. 76:1393–1421.
10. Cauda V, Pugliese D, Garino N, Sacco A, Bianco S, et al. (2014) Multi-functional energy conversion and storage electrodes using flower like zinc oxide nanostructures. Energy. 65:639–646.
11. Chen T, Liu W, Zhuo Y, Hu H, Zhu M, (2020) Single phase P2-type layered oxide with Cu-substitution for sodium ion batteries. J Energy Chem. 43:148–154.
12. Cheng CA, Deng T, Lin FC, Cai Y, Zink JI (2019) Supramolecular nanomachines as stimuli-responsive gatekeepers on mesoporous silica nanoparticles for antibiotic and cancer drug delivery. Theranostics. 9(11): 1-24.
13. Emeline A, Ryabchuk V, Serpone N (2007) Photoreactions occurring on metal oxide surfaces are not all

photocatalytic: Description of criteria and conditions for processes to be photocatalytic. Catal Today. 122:91–100.

14. Essawy AA (2018) Silver imprinted zinc oxide nanoparticles: Green synthetic approach, characterization and efficient sunlight induced photocatalytic water detoxification. J Clean Prod. 183:1011-1020.
15. Gionco C, Fabbri D, Calza P, Paganini MC (2016) Synthesis, characterization, and photocatalytic tests of N-doped zinc oxide: A new interesting photocatalyst. J Nanomater. 16:1-8.
16. Gupta SM, Tripathi M (2012) An overview of commonly used semiconductor nanoparticles in photocatalysis. High Energy Chem. 46:1–9.
17. Gupta VK, Ali I, Saleh TA, Nayak A, Agarwal S (2012) Chemical treatment technologies for waste-water recycling an overview. Rsc Adv. 2:6380–6388.
18. Huang B, Zhang Z, Zhao C, Cairang L, Bai J, et al. (2018) Enhanced gas sensing performance of SnO. $In2O_3$ core@ shell nanofibers prepared by coaxial electrospinning. Sens Actuators B Chem. 255:2248–2257.
19. Jang JS, Kim J, Ghorpade U, Shin HH, Gang MG, et al. (2019) Comparison study of SnO based quaternary TCO materials for photovoltaic application. J Alloy Compd. 793:499–504.
20. Jiang D, Xing C, Liang X, Shao L, Chen M (2016) Synthesis of cuprous oxide with morphological evolution from truncated octahedral to spherical structures and their size and shape-dependent photocatalytic activities. J Colloid Interface Sci. 461:25-31.